RAA 2016 Vol. **16** No. **4**, 62 (8pp) doi: 10.1088/1674–4527/16/4/062
http://www.raa-journal.org *http://iopscience.iop.org/raa*

Research in Astronomy and Astrophysics

Jet-dominated quiescent state in black hole X-ray binaries: the cases of A0620–00 and XTE J1118+480

Qi-Xiang Yang

Key Laboratory for Research in Galaxies and Cosmology, Shanghai Astronomical Observatory, Chinese Academy of Sciences, Shanghai 200030, China; *qxyang@shao.ac.cn*
University of Chinese Academy of Sciences, Beijing 100049, China

Received 2015 September 17; accepted 2015 October 24

Abstract The radiative mechanism of black hole X-ray transients (BHXTs) in their quiescent states (defined as the 2–10 keV X-ray luminosity $\lesssim 10^{34}\,\mathrm{erg\,s^{-1}}$) remains unclear. In this work, we investigate the quasi-simultaneous quiescent state spectrum (including radio, infrared, optical, ultraviolet and X-ray) of two BHXTs, A0620–00 and XTE J1118+480. We find that these two sources can be well described by a coupled accretion – jet model. More specifically, most of the emission (radio up to infrared, and the X-ray waveband) comes from the collimated relativistic jet. Emission from hot accretion flow is totally insignificant, and it can only be observed in mid-infrared (the synchrotron peak). Emission from the outer cold disk is only evident in the UV band. These results are consistent with our previous investigation on the quiescent state of V404 Cyg and confirm that the quiescent state is jet-dominated.

Key words: accretion, accretion disks — black hole physics — X-rays: binaries — stars: jets — stars: individual (A0620–00, XTE J1118+480)

1 INTRODUCTION

Black hole X-ray transients (BHXTs) are binary systems in which the black hole accretes matter from its companion. For the majority of time, BHXTs are observed to be extraordinarily faint, with X-ray (in the energy band 2–10 keV) luminosity $L_{\rm X} \lesssim 10^{34}\ \mathrm{erg\,s^{-1}} \lesssim 10^{-5}\ L_{\rm Edd}$.[1] Terminologically, this faint period is called the "quiescent state." Such a faint accretion phase is also observed in accretion systems around supermassive black holes (SMBHs), i.e. most of the nearby active galactic nuclei (AGNs) are systems accreting at low luminosities, with $L_{\rm X} \lesssim 10^{-6}\ L_{\rm Edd}$ (e.g. Ho 2008, 2009; Pellegrini 2010). It is further argued that most SMBHs remain non-active during their lifetime.

Occasionally, with long intervals (years to decades) staying in a quiescent state, BHXTs will undergo outbursts, during which they exhibit distinctive states (soft, hard and intermediate) according to the spectral and timing properties (Zdziarski & Gierliński 2004; Homan & Belloni 2005; Remillard & McClintock 2006; Done et al. 2007; Belloni 2010), likely a consequence of the changes in accretion modes (e.g. Esin et al. 1997). It is now widely accepted that the spectrum of the soft state can be described by a cold multi-temperature blackbody emission, i.e. the accretion flow is a geometrically-thin Shakura-Sunyaev disk (Shakura & Sunyaev 1973, hereafter SSD) extending down to the innermost stable circular orbit (ISCO). Hot corona sandwiching the SSD will emit power-law X-ray spectra. The accretion flow and the radiative mechanism of the hard state, on the other hand, is still under active debate. Several models with different dynamics are proposed, i.e. the maximally efficient jet model (Markoff et al. 2005; Kylafis et al. 2008), the jet-emitting-disk model (e.g. Ferreira et al. 2006; Zhang & Xie 2013), the evaporated-corona model (Liu et al. 2002, 2007; Qiao & Liu 2013), and finally our favorite, the accretion – jet model (Esin et al. 1997; Yuan et al. 2005, hereafter YCN05. See Yuan & Narayan 2014 for an up-to-date review on this model). More details on the accretion – jet model will be given later in Section 3. Moreover, the collimated relativistic jet, which is most evident in the radio band, is also observed to be correlated with the accretion mode (e.g. Fender et al. 2004). It is evident in the hard state but will be highly suppressed during the soft state.

Compared to soft and hard states, the nature of the quiescent states in BHXTs remains even more unclear (Narayan et al. 2002; Narayan & McClintock 2008; Xie et al. 2014, hereafter XYM14; Plotkin et al. 2015). Extensive efforts have been devoted to understanding the quiescent state of BHXTs during the past decade. Observationally, it is well known that the X-ray spectrum of the quiescent state is much softer than hard states, when the photon index Γ (defined as the flux at given

[1] The Eddington luminosity is $L_{\rm Edd} = 1.3 \times 10^{38} (M_{\rm BH}/M_\odot)$ erg s^{-1}, where $M_{\rm BH}$ is the black hole mass.

frequency $F_\nu \propto \nu^{1-\Gamma}$) plateaus to an average $\langle\Gamma\rangle \approx 2.1$ (Kong et al. 2002; Corbel et al. 2006; Pszota et al. 2008; Reynolds & Miller 2011; Plotkin et al. 2013; Reynolds et al. 2014; Bernardini & Cackett 2014; Yang et al. 2015). These observations indicate that the quiescent state may be different from the hard states in terms of its radiative mechanism. Moreover, the optical and X-ray variabilities in the quiescent state are tightly correlated (Hynes et al. 2004; Reynolds & Miller 2011. See XYM14 for a theoretical interpretation.), e.g. in V404 Cyg. Moreover, recently it has been found that the quiescent state of BHXTs is not silent or quiet as expected, but instead shows numerous weak activities (e.g. Cantrell et al. 2010; Khargharia et al. 2013; Bernardini & Cackett 2014; Rana et al. 2015).

Theoretically, several models have been proposed for X-ray emission in the quiescent state. It could be the synchrotron radiation from the non-thermal electrons in the jet (e.g. Yuan & Cui 2005; Pszota et al. 2008), or the Comptonized emission with seed photons (synchroton) in an advection-dominated accretion flow (ADAF, e.g. Narayan et al. 1996, 1997), or the synchrotron self-Compton (SSC) processes with seed photons emitted by a quasi-thermal population of relativistic electrons (e.g. Gallo et al. 2007; Plotkin et al. 2015). In the accretion – jet scenario which achieved great success in the hard states of BHXTs (Yuan & Narayan 2014), it is shown that the X-ray emission of the quiescent state of BHXTs will be the optically thin synchrotron emission from the jet rather than the hot accretion flow (e.g. Yuan & Cui 2005; Pszota et al. 2008; XYM14). This prediction is supported by several observations (see XYM14 for a recent summary).

(1) The quiescent-state spectral energy distribution (SED) of individual sources can be well modeled by the jet theory (Pszota et al. 2008; XYM14).
(2) Deep *XMM-Newton* X-ray observations with high signal-to-noise (S/N) ratio, on sources V404 Cyg, GRO J1655–40 and XTE J1550–564 (less confirmative due to relatively poorer S/N ratio), indicate that their X-ray spectra are precisely power-law, without any curvatures (Pszota et al. 2008).
(3) Statistically, the value of X-ray photon index of the quiescent state is roughly constant, independent of the X-ray luminosity (Plotkin et al. 2013; Yang et al. 2015).

In addition, through fitting the SEDs in extremely low-luminosity active galactic nuclei (LLAGNs), it is also shown that the X-ray spectrum of those 'quiescent' AGNs could be well fitted by the jet model (e.g. Wu et al. 2007; Yuan et al. 2009; Yu et al. 2011).

We in this work aim to provide additional support to the jet scenario of the quiescent state of BHXTs. In Section 2 we first give the backgrounds and observations of the two sources investigated here, A0620–00 and XTE J1118+480, with a focus on the quasi-simultaneous multi-band (from radio to X-ray) observations in their quiescent states.

We note that both sources have been modeled under the maximally efficient jet model (A0620–00: Gallo et al. 2007. XTE J1118+480: Plotkin et al. 2015). Subsequently in Section 3 we describe the accretion – jet model we used, and then in Section 4 provide a comprehensive multi-band spectral fitting of the spectra. The last section is devoted to discussions and a brief summary.

2 OBSERVATIONS OF QUIESCENT STATES OF BHXTS

2.1 Observations of A0620–00 in Quiescent State

A0620–00, discovered in 1975, is a low-mass X-ray binary which has been in quiescent state for almost 40 years. As summarized in Table 1, it is located at a distance $d = 1.06 \pm 0.12\,\mathrm{kpc}$ (Cantrell et al. 2010). The orbital period is $P_{\rm orb} = 7.75\,\mathrm{h}$ (Johannsen et al. 2009) and the line-of-sight inclination angle of the binary system is also constrained to be $\theta = 51.0^\circ \pm 0.9^\circ$. The mass and spin of the black hole are, respectively, $M_{\rm BH} = 6.6 \pm 0.25\ M_\odot$ (Cantrell et al. 2010) and $a_* = 0.12 \pm 0.19$ (Gou et al. 2010). The mass and size of the companion star are respectively $0.40\ M_\odot$ and $0.56\ R_\odot$. In addition, the companion has a spectral type K5V with a temperature of 4400 K (Cantrell et al. 2010).

To our knowledge, there are two broadband nearly-simultaneous observations on this source, at X-ray luminosity $L_{\rm X} \sim 10^{-8.5}\ L_{\rm Edd}$. The first is in August, 2005 (Gallo et al. 2007), where they focused on the *Spitzer* observation. Later, on 2010 March 23–25, Froning et al. (2011) carried out contemporaneous X-ray (by *Swift*/XRT), ultraviolet (UV, by HST/COS, HST/STIS and *Swift*/UVOT), optical (by *Swift*/UVOT and SMARTS/ANDICAM), near-infrared (NIR, by Keck and SMARTS/ANDICAM), and radio (by ATCA) observations. For details on both instruments involved and data reduction, the readers are referred to Froning et al. (2011). We also compile the infrared (IR) *WISE* observation of this source, which was observed on 2010 March 19, i.e. only one week earlier (Wang & Wang 2014). The observational data are shown in the left panel of Figure 1. We have two notes here.

First, there are too few photons detected by *Swift*/XRT to constrain the X-ray photon index. We can only adopt Γ from previous sensitive observations, by e.g. *Chandra*, with similar X-ray fluxes (see Froning et al. 2011 for more details).

Second, the ATCA radio observations at 5.5 GHz and 9 GHz are only upper limits. Again, we utilize data from Gallo et al. (2007), which have similar IR and X-ray fluxes to the new observations, as compensatory data.

Table 1 Basic Properties of Individual Sources

Sources	Distance d (kpc)	Black hole mass $M_{\rm BH}$ ($M_\odot$)	Orbital period $P_{\rm orb}$ (h)	Inclination θ (°)	Binary separation a (cm)	Companion star (MK Type, Temperature, Radius)	Ref.
A0620–00	1.06 ± 0.12	6.6 ± 0.25	7.75	51.0 ± 0.9	2.6×10^{11}	K5V, 4400 K, $0.50 - 0.56\ R_\odot$	J09, C10
XTE J1118+480	1.72 ± 0.10	7.5 ± 0.6	4.08	$68 - 79$	1.8×10^{11}	K7V–M1V, 4000 K, $0.6\ R_\odot$	T04, G06, K13

Notes: References: T04 – Torres et al. (2004); G06 – Gelino et al. (2006); J09 – Johannsen et al. (2009); C10 – Cantrell et al. (2010); K13 – Khargharia et al. (2013).

2.2 Observations of XTE J1118+480 in Quiescent State

XTE J1118+480, discovered by the *Rossi X-Ray Timing Explorer* (*RXTE*) all-sky monitor on 2000 March 29, is a low-mass X-ray binary that has undergone several outbursts. As summarized in Table 1, it is located at a distance $d = 1.72 \pm 0.10$ kpc (Gelino et al. 2006), with a black hole mass $M_{\rm BH} = 7.5 \pm 0.6\ M_\odot$ (Khargharia et al. 2013). The orbital period is $P_{\rm orb} = 4.08$ h (Torres et al. 2004) and the line-of-sight inclination angle of the binary system is also constrained to be $\theta = 68^\circ - 79^\circ$ (Khargharia et al. 2013). The mass and size of the companion star are respectively $0.3 \pm 0.2\ M_\odot$ (Mirabel et al. 2001) and $0.6\ R_\odot$. In addition, the companion has a spectral type K7V–M1V with a temperature of 4000 K (Khargharia et al. 2013).

Broadband nearly-simultaneous observations of XTE J1118+480 were carried out on 2013 June 27–28 (Gallo et al. 2014; Plotkin et al. 2015). Wavebands included in these observations are X-ray (by *Chandra*/ACIS), ultraviolet (by *Swift*/UVOT), optical (by WHT/ACAM), NIR (by WHT/LIRIS and 2MASS), and radio (by VLA). For details on both instruments involved and the related data reduction, readers are referred to Plotkin et al. (2015). Note that we also have compiled mid-IR (by *WISE*) observations of this source in quiescent state on 2010 March 10 (Wang & Wang 2014). The observational data of XTE J1118+480 in its quiescent state are shown in the right panel of Figure 1.

3 THE ACCRETION – JET MODEL

In this work, we take the accretion – jet model, which has been successfully applied to BHXTs in their hard states and LLAGNs (see Yuan & Narayan 2014 for a recent review). In this model, three components are considered (YCN05), i.e. an outer (possibly irradiated) SSD, which has an outer boundary $R_{\rm out,SSD}$ and will be truncated at radius $R_{\rm tr}$, an inner hot accretion flow within $R_{\rm tr}$, and finally a collimated relativistic jet perpendicular to the plane of the accretion flow. From an observational point of view, the three components of the accretion – jet model are prominent in different wavebands. Very roughly, the truncated SSD, the hot accretion flow and the jet, respectively, contribute mainly to the radiation in the IR–UV, X-ray and radio bands.

In the following subsection, we provide more detailed information about the accretion-jet model, especially the jet component, since we support the position that most of the X-ray radiation is the synchrotron emission from the jet (see Yuan & Cui 2005; Pszota et al. 2008; XYM14).

3.1 Hot Accretion Flow Model

The hot accretion flow adopted in our model is an ADAF (Narayan & Yi 1994). Compared with the ADAF model adopted in Narayan et al. (1996), two important issues are taken into account (see Xie & Yuan 2012; Yuan & Narayan 2014 for summaries), i.e. the existence of outflow and the viscous/turbulent heating onto electrons. For the outflow, both observational evidence and theoretical simulations find that strong wind exists in the hot accretion flow (Yuan et al. 2012a; Yuan & Narayan 2014; Yuan et al. 2015). Consequently, the accretion rate follows $\dot{M}(R) \propto R^s$, where index s is the outflow parameter, ranging from ~ 0.4 to ~ 0.8 (Yuan et al. 2012b).

The fraction of turbulent viscous/turbulent heating rate that goes into electrons is designated as δ. The microphysics of viscous/turbulent heating is still under active research and numerous processes have been proposed, i.e. MHD turbulence (Quataert 1998; Blackman 1999; Lehe et al. 2009), magnetic reconnection (Bisnovatyi-Kogan & Lovelace 1997; Quataert & Gruzinov 1999; Ding et al. 2010), or dissipation of pressure anisotropy (Sharma et al. 2007; Sironi & Narayan 2015). Different microphysics will result in different values of δ, and it is likely in the range from 0.1 to 0.5 (see Yuan & Narayan 2014). Throughout this work, we adopt $\delta = 0.1$ in our numerical calculations (Yang et al. 2015).

3.2 Jet Model

Our jet model is phenomenological (see YCN05, Xie & Yuan 2015 for more details). The composition is assumed to be normal plasma, i.e. electrons and protons. The bulk Lorentz factor of the compact jet is set to $\Gamma_{\rm jet} = 1.2$, a

typical value for the jets in the hard state of BHXTs (Gallo et al. 2003; Fender 2006). The opening angle is $\theta_{\rm jet} = 0.1$ (or equivalently $\theta_{\rm jet} \sim 5.7^\circ$).

Within the jet itself, different shells of moving plasma are assumed to have different velocities. When the faster but later shells catch up with the slower and earlier ones, internal shocks occur. The spatial filling factor of the internal shock shells is assumed to be 0.1. In these internal shocks a fraction (ξ) of the electrons will be accelerated into a power-law energy distribution, with an index of $p_{\rm e}$. Due to the strong radiative cooling, the high-energy part (self-consistently determined in our calculations) of the accelerated power-law electrons will be cooled down, and their distribution index will be $p_{\rm e}+1$ (Rybicki & Lightman 1979). Two additional parameters, ϵ_e and $\epsilon_{\rm B}$, are also included to quantify the fraction of the shock energy that goes into electrons and magnetic fields, respectively. For simplicity, all these microphysical parameters are assumed to be constant along the jet direction.

With the above parameters, we can calculate the synchrotron emission from these accelerated power-law electrons. The parameter dependence is extensively discussed in XYM14. The SED of the jet (or more generally the power-law electrons) in general is fairly simple. The high energy part (e.g. UV and X-ray bands) follows a power-law, with photon index $\Gamma \approx 1+(p_{\rm e}+1-1)/2 = 1+p_{\rm e}/2$ (Rybicki & Lightman 1979). The spectrum of the low energy part (e.g. radio up to IR) also follows a power-law, but is flat or slightly inverted because of self-absorption.

4 RESULTS

Before presenting our results, we first comment on the ADAF model for the quiescent state (e.g., Narayan et al. 1996, 1997), where the X-ray radiation is believed to be emitted from ADAF. Observationally, the ADAF model suffers two problems. First, once the X-ray flux is fitted, the UV (with $\nu \gtrsim 10^{15}$ Hz) emission predicted by the ADAF model is substantially higher compared to observations (fig. 1a in Yuan & Narayan 2014 for the spectrum of ADAF at low accretion rate). This argument is adopted by Hynes et al. (2009) for the observation of V404 Cyg in its quiescent state, where they found that the ADAF model produces too strong UV emission, by a factor of ~ 10, for a given X-ray flux. Second, the radio observation of the quiescent state indicates the existence of a jet, or, more generally, non-thermal electrons. These non-thermal electrons are also likely to emit in the X-ray band, i.e. the jet contribution in the X-ray band should be taken into account. Because of the above two reasons, the ADAF model seems unlikely.

We thus apply the accretion – jet model to fit the quasi-simultaneous multi-band observations of both A0620–00 and XTE J1118+480. Below we detail our methods and results.

We first take into account emission from the companion star. We adopt the stellar atmosphere model by Kurucz (1993). As shown by the blue dotted curves in Figure 1, the companion dominates the radiation in mid-IR-optical bands.

We secondly constrain the jet emission contribution. Observationally, the X-ray emission of the quiescent state can be fitted by a power-law, i.e. with photon index of $\Gamma = 2.26 \pm 0.18$ (McClintock et al. 2003; it has similar X-ray flux as this observation) for A0620–00 and $\Gamma = 2.02 \pm 0.41$ (Plotkin et al. 2015) for XTE J1118+480. Extending the power-law spectrum to a lower energy band (e.g. UV with $\nu \sim 10^{15}$ Hz), we find that it can naturally compensate the excess emission in UV. For the value of Γ in both sources, we pre-fix in our jet model $p_{\rm jet} = 2.3$, a value consistent with the diffusive shock acceleration theory. There are four free parameters left, $\dot{M}_{\rm jet}$, ξ, ϵ_e and $\epsilon_{\rm B}$ (see XYM14 for discussions on the effects of these parameters). Through spectral modeling (i.e. fluxes in radio, IR, UV and X-ray bands), we can obtain the physical parameters of the fitting (listed in Table 2), which are all within the typical range obtained in a GRB afterglow (YCN05). We find that radiation in mid-UV up to X-ray bands is the optically thin part of the synchrotron radiation. On the other hand, the radiation in radio up to far-IR bands is the optically thick self-absorbed synchrotron radiation, and the spectrum is flat with spectral index $\alpha_{R-IR} \approx 0$.

Thirdly, we check the radiative contribution from the inner hot accretion flow and the outer cold disk. Generally the radiation from the outer cold disk is difficult to constrain in quiescent states, due to the dominance of the companion star, e.g. the case in V404 Cyg (XYM14). However, the emission of the bluer-optical band up to the UV band of A0620–00 and XTE J1118+480 in their quiescent states shows clear flux excess compared to that from the companion (Fig. 1). Such excess can be understood naturally as emission from the outer cold disk. We considered the irradiated cold disk model, with three model parameters, i.e. the accretion rate ($\dot{M}_{\rm SSD}$), and the outer and inner radii ($R_{\rm out,SSD}$ and $R_{\rm in,SSD}$ respectively; note that $R_{\rm in,SSD} \equiv R_{\rm tr}$). We emphasize that the SED coverage in the UV band is of crucial importance to determine the transition radius $R_{\rm tr}$. Emission from the outer irradiated cold disk is shown as green dot-dashed curves in Figure 1.

Subsequently, we assume that the mass-loss rate in the jet ($\dot{M}_{\rm jet}$) at $5R_{\rm s}$ (here $R_{\rm s}$ is the Schwarzschild radius of the black hole) is $\sim 6\%$ of the accretion rate at $5R_{\rm s}$, a reasonable value in the coupled accretion – jet model (see e.g. fig. 2 in Yuan & Cui 2005). With the accretion rates at $R_{\rm tr}$ and $5R_{\rm s}$, the outflow parameter s can then be constrained, i.e. $s \approx 0.4$ for A0620–00 and $s \approx 0.6$ for XTE J1118+480. Both values are consistent with the suggested range ($s \sim 0.4-0.8$) from recent large-scale numerical simulations of hot accretion flows (e.g. Yuan et al. 2012b). Other basic parameters

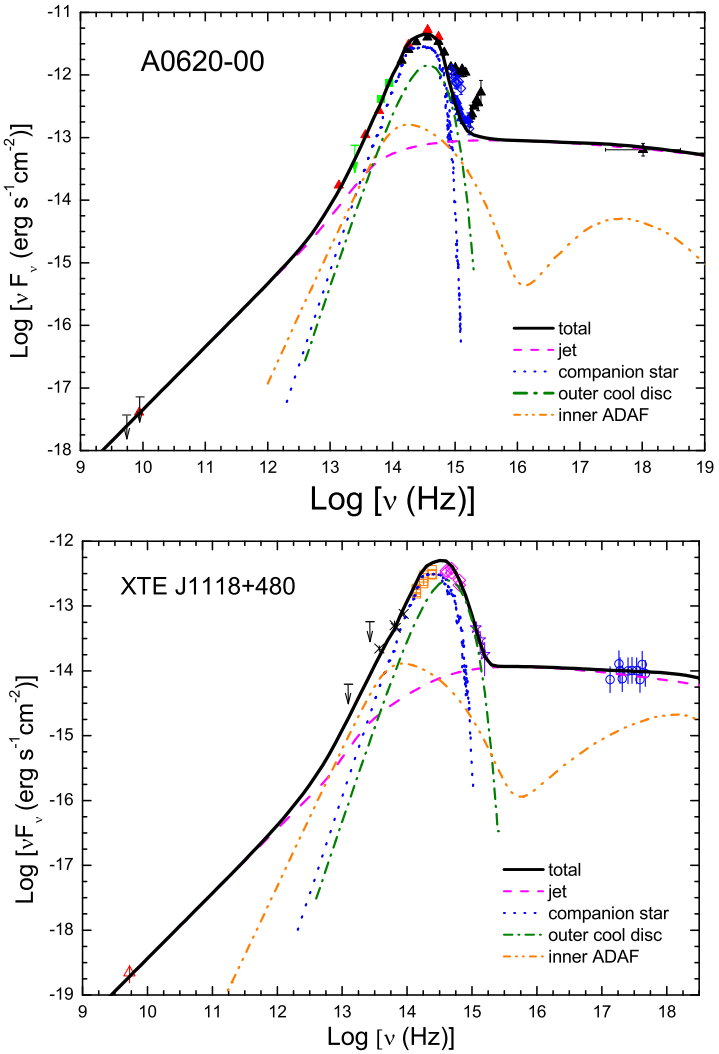

Fig. 1 Broadband SED and the spectral fitting results (curves labeled) of two BHXBs (A0620–00 and XTE J1118+480) in their quiescent states. *Top*: A0620–00. The solid black triangles are from nearly-simultaneous observation by Froning et al. (2011), while the solid red triangles and green squares show the non-simultaneous data from Gallo et al. (2007) and Wang & Wang (2014), respectively. *Bottom*: XTE J1118+480. The observational data are taken from Plotkin et al. (2015). Symbols are for the radio (*triangle*), (non-simultaneous) IR (arrows for upper limits; crosses for detections), NIR and optical (*squares*), UV (*stars*), and X-ray (*circles*) data points.

Table 2 Modeling Parameters of the Coupled Accretion – Jet Model

Sources	$\dot{M}_{\rm SSD}$ ($10^{-4}\ \dot{M}_{\rm Edd}$)	$R_{\rm out,SSD}$ ($10^4\ R_{\rm s}$)	$R_{\rm tr}$ ($10^4\ R_{\rm s}$)	s	$\dot{M}_{\rm jet}$ ($10^{-6}\ \dot{M}_{\rm Edd}$)	$p_{\rm e}$	$\epsilon_{\rm e}$	$\epsilon_{\rm B}$	ξ
A0620–00	4.0	2.5	1.0	0.4	1.2	2.3	0.01	0.04	0.06
XTE J1118+480	6.0	2.0	0.8	0.6	0.43	2.3	0.025	0.05	0.04
V404 Cyg	50.0	5.0	2.0	0.6	3.0	2.4	0.04	0.03	0.08

of the hot accretion flow include the viscous parameter $\alpha_{\rm vis} = 0.3$, the magnetic parameter (defined as the ratio of the gas to magnetic pressure) $\beta = 9$, and the fraction of viscous heating onto electrons $\delta = 0.1$ (Yang et al. 2015). Emission from the inner ADAF is shown as dot-dot-dashed curves in Figure 1, where the lower-ν peak is the synchrotron and the higher-ν peak is bremsstrahlung (dominated) with a negligible fraction of inverse Compton. Evidently from Figure 1, emission from ADAF is not important at any wavebands for the quiescent state of BHXTs (also see XYM14).

We summarize the detailed modeling parameters of the coupled accretion – jet model for the quiescent state of A0620–00 and XTE J1118+480, and list them in Table 2.

For comparison and completeness, we also list the fitting parameters of V404 Cyg in its quiescent state (XYM14). Obviously the fitting parameters from these three BHXTs are quite similar to each other.

We note that independent estimation and/or measurement of both $R_{\rm tr}$ and $\dot{M}_{\rm SSD}$ has been developed. For example, the transition radius $R_{\rm tr}$ can be estimated from the low frequency (roughly at mHz level) quasi-periodic oscillation (QPO). For XTE J1118+480, Shahbaz et al. (2005) carried out high time-resolution multi-color ULTRACAM observation of this source in its quiescent state, which has similar X-ray flux to the observations adopted here, and found that the power density spectrum of the light curves could be described by a power-law model plus a broad QPO with frequency $\sim$ 2 mHz. Assuming it is the Keplerian rotational frequency at the transition radius (Giannios & Spruit 2004), they estimated $R_{\rm tr} \approx 8000\ R_{\rm s}$, consistent with the value derived from spectral fitting.

Lasota (2000) provided a formula to estimate mass accretion rate at large radius for systems in their quiescent state, i.e.

$$\dot{M}(R) \approx 4.0\times10^{15}\,(M_{\rm BH}/1\ M_\odot)^{-0.88} \times \left(R/10^{10}\ {\rm cm}\right)^{2.65}\ {\rm g\ s^{-1}}\,.$$

Applying the formula to A0620–00 and XTE J1118+480, we find the accretion rates of the outer cold disk are, respectively, $\approx 5\times10^{-4}\ \dot{M}_{\rm Edd}$ and $\approx 3\times10^{-4}\ \dot{M}_{\rm Edd}$, where $\dot{M}_{\rm Edd} = 10\ L_{\rm Edd}/c^2$ is the Eddington accretion rate. Again, these values are consistent, within a factor of $\sim$ 2, with the values from spectral modeling results (Table 2).

5 SUMMARY AND DISCUSSION

The radiative properties of the quiescent state, either in BHXTs or in normal galaxies, remain unclear, and numerous efforts have been devoted to this field. Thanks to the high-sensitivity X-ray telescopes and the joint multi-band (quasi-)simultaneous observations, together with long-term narrow-band monitoring, we confirm previous theoretical results (see XYM14 for summaries) that the emission of the quiescent states of BHXTs is dominated by radiation from the compact relativistic jet. The outer thin disk and the inner hot accretion flow generally play negligible roles in radiation, while the companion dominates the emission between mid-IR and optical bands. We also illustrate that the jet-dominated quiescent state model can explain most of the observational features (see XYM14 for details). Below we provide several discussions of our results.

5.1 The UV Spectrum of A6020–00

Froning et al. (2011) in their *Hubble* observations, include both the near-UV (NUV; $\nu < 1.5\times10^{15}$ Hz) STIS instrument and far-UV (FUV; $\nu > 1.5\times10^{15}$ Hz) COS instrument. However, clear discrepancies between these two instruments are observed (see the left panel in Fig. 1), i.e. the FUV spectrum is rather blue (flux $F_\nu \propto \nu^{-\alpha}$, with $\alpha > -1$). Besides, the NUV spectrum, which is also moderately blue, is also different from previous observation.

The UV spectrum is discussed extensively in Froning et al. (2011). More directly, they fitted this part with a new thermal component, and found it moderately hot and compact, with temperature $\sim 10^4$ K and size $\sim 4\times10^9$ cm. Several possibilities have been proposed; most likely it is the bright spot (the accretion stream-disk impact point). It can also be related to the transition zone (close to the transition radius) between the outer cold disk and the inner hot accretion flow. In the current work, we do not include this complexity.

5.2 Radio/X-ray Correlation in Quiescent State

One important but unclear question is the correlation coefficient between the radio luminosity and X-ray luminosity, in the form $L_R \propto L_X^p$, where p is the correlation coefficient, in quiescent state of black hole sources. Tight and strong radio/X-ray correlation is observed in both AGNs and BHXTs (e.g. Merloni et al. 2003; Corbel et al. 2013), with $p \approx 0.6$. Under the accretion – jet model, Yuan & Cui (2005) theoretically predict that the correlation will steepen, with $p \sim 1.23$, when the X-ray luminosity $L_{\rm X}$ is below a critical value, $L_{\rm X,crit} \sim 10^{-5} - 10^{-6}\ L_{\rm Edd}$ ($L_{\rm Edd}$ is the Eddington luminosity), where the X-ray emission will come from the jet rather than the hot accretion flow normally observed in the hard/bright states (Yuan & Cui 2005). This prediction is confirmed by later works, i.e., data from all available LLAGNs satisfying $L_{\rm X} \lesssim L_{\rm X,crit}$ follow $L_R \propto L_{\rm X}^{1.22}$ (Pellegrini et al. 2007; Wu et al. 2007; Wrobel et al. 2008; Yuan et al. 2009; de Gasperin et al. 2011; Younes et al. 2012).

In the case of BHXTs, however, the answer is not so clear. We here emphasize two cautions. First, although the observations of A0620–00 and XTE J1118+480 can be fitted well within the jet model for the combined data set (Sect. 4), the radio data are still not very good/robust (see also Yuan & Narayan 2014). For example, the most recent radio detection of XTE J1118+480 in its quiescent state is marginal, only at a 3σ level (Gallo et al. 2014), while A0620–00 is an underdetection (Froning et al. 2011) or also at a 3σ level (Gallo et al. 2007).

Second, there might be systematical differences between low-luminosity AGNs and BHXTs, in the sense of a different mass supply. The BHXTs accrete material from their companion, where the binary separation will constrain the size and location of the outer cold disk (Table 1). Consequently the jet properties ($\Gamma_{\rm jet}, \xi, \epsilon_e, \epsilon_{\rm B}$) and their relationship with the decreasing mass loss rate into the jet $\dot{M}_{\rm jet}$ in BHXTs and AGNs may be different.

One direct piece of evidence is that the bulk Lorentz factor of the compact jet in BHXTs is $\Gamma_{\rm jet} \lesssim 1.6$ (e.g. Fender et al. 2004), while it is likely much higher in AGNs, with a typical value of $\Gamma_{\rm jet} \sim 10$. Besides, the magnetic field configuration in BHXTs may also be different from that in AGNs, which may also eventually affect the jet formation/acceleration processes. Further efforts, both theoretical and observational, are still needed to understand the physics of jets.

Acknowledgements QXY is grateful to the anonymous referee for constructive suggestions, and Prof. Feng Yuan, Dr. Fu-Guo Xie and Yaping Li for useful discussions. This work was supported by the National Basic Research Program of China (973 Program, Grant 2014CB845800), the National Natural Science Foundation of China (Grant Nos. 11203057, 11103061, 11133005 and 11121062), and the Strategic Priority Research Program "The Emergence of Cosmological Structures" of the Chinese Academy of Sciences (Grant XDB09000000).

References

Belloni, T. M. 2010, in Lecture Notes in Physics, 794, ed. T. Belloni, 53 (Berlin: Springer Verlag)
Bernardini, F., & Cackett, E. M. 2014, MNRAS, 439, 2771
Bisnovatyi-Kogan, G. S., & Lovelace, R. V. E. 1997, ApJ, 486, L43
Blackman, E. G. 1999, MNRAS, 302, 723
Cantrell, A. G., Bailyn, C. D., Orosz, J. A., et al. 2010, ApJ, 710, 1127
Corbel, S., Coriat, M., Brocksopp, C., et al. 2013, MNRAS, 428, 2500
Corbel, S., Tomsick, J. A., & Kaaret, P. 2006, ApJ, 636, 971
de Gasperin, F., Merloni, A., Sell, P., et al. 2011, MNRAS, 415, 2910
Ding, J., Yuan, F., & Liang, E. 2010, ApJ, 708, 1545
Done, C., Gierliński, M., & Kubota, A. 2007, A&A Rev., 15, 1
Esin, A. A., McClintock, J. E., & Narayan, R. 1997, ApJ, 489, 865
Fender, R. P., Belloni, T. M., & Gallo, E. 2004, MNRAS, 355, 1105
Fender, R. 2006, Jets from X-ray Binaries, in Compact Stellar X-ray Sources, eds. W. H. G. Lewin, & M. van der Klis, 381 (Cambridge: Cambridge Univ. Press)
Ferreira, J., Petrucci, P.-O., Henri, G., Saugé, L., & Pelletier, G. 2006, A&A, 447, 813
Froning, C. S., Cantrell, A. G., Maccarone, T. J., et al. 2011, ApJ, 743, 26
Gallo, E., Fender, R. P., & Pooley, G. G. 2003, MNRAS, 344, 60
Gallo, E., Migliari, S., Markoff, S., et al. 2007, ApJ, 670, 600
Gallo, E., Miller-Jones, J. C. A., Russell, D. M., et al. 2014, MNRAS, 445, 290
Gelino, D. M., Balman, Ş., Kızıloğlu, Ü., et al. 2006, ApJ, 642, 438
Giannios, D., & Spruit, H. C. 2004, A&A, 427, 251
Gou, L., McClintock, J. E., Steiner, J. F., et al. 2010, ApJ, 718, L122
Ho, L. C. 2008, ARA&A, 46, 475
Ho, L. C. 2009, ApJ, 699, 626
Homan, J., & Belloni, T. 2005, Ap&SS, 300, 107
Hynes, R. I., Bradley, C. K., Rupen, M., et al. 2009, MNRAS, 399, 2239
Hynes, R. I., Charles, P. A., Garcia, M. R., et al. 2004, ApJ, 611, L125
Johannsen, T., Psaltis, D., & McClintock, J. E. 2009, ApJ, 691, 997
Khargharia, J., Froning, C. S., Robinson, E. L., & Gelino, D. M. 2013, AJ, 145, 21
Kong, A. K. H., McClintock, J. E., Garcia, M. R., Murray, S. S., & Barret, D. 2002, ApJ, 570, 277
Kurucz, R. L. 1993, SYNTHE Spectrum Synthesis Programs and Line Data (Cambridge, MA: Smithsonian Astrophysical Observatory)
Kylafis, N. D., Papadakis, I. E., Reig, P., Giannios, D., & Pooley, G. G. 2008, A&A, 489, 481
Lasota, J.-P. 2000, A&A, 360, 575
Lehe, R., Parrish, I. J., & Quataert, E. 2009, ApJ, 707, 404
Liu, B. F., Mineshige, S., Meyer, F., Meyer-Hofmeister, E., & Kawaguchi, T. 2002, ApJ, 575, 117
Liu, B. F., Taam, R. E., Meyer-Hofmeister, E., & Meyer, F. 2007, ApJ, 671, 695
Markoff, S., Nowak, M. A., & Wilms, J. 2005, ApJ, 635, 1203
McClintock, J. E., Narayan, R., Garcia, M. R., et al. 2003, ApJ, 593, 435
Merloni, A., Heinz, S., & di Matteo, T. 2003, MNRAS, 345, 1057
Mirabel, I. F., Dhawan, V., Mignani, R. P., Rodrigues, I., & Guglielmetti, F. 2001, Nature, 413, 139
Narayan, R., Barret, D., & McClintock, J. E. 1997, ApJ, 482, 448
Narayan, R., Garcia, M. R., & McClintock, J. E. 2002, in The Ninth Marcel Grossmann Meeting, ed. V. G. Gurzadyan, R. T. Jantzen, & R. Ruffini, 405
Narayan, R., & McClintock, J. E. 2008, New Astron. Rev., 51, 733
Narayan, R., McClintock, J. E., & Yi, I. 1996, ApJ, 457, 821
Narayan, R., & Yi, I. 1994, ApJ, 428, L13
Pellegrini, S. 2010, ApJ, 717, 640
Pellegrini, S., Siemiginowska, A., Fabbiano, G., et al. 2007, ApJ, 667, 749
Plotkin, R. M., Gallo, E., & Jonker, P. G. 2013, ApJ, 773, 59
Plotkin, R. M., Gallo, E., Markoff, S., et al. 2015, MNRAS, 446, 4098
Pszota, G., Zhang, H., Yuan, F., & Cui, W. 2008, MNRAS, 389, 423
Qiao, E., & Liu, B. F. 2013, ApJ, 764, 2
Quataert, E. 1998, ApJ, 500, 978

Quataert, E., & Gruzinov, A. 1999, ApJ, 520, 248
Rana, V., Loh, A., Corbel, S., et al. 2015, arXiv:1507.04049
Remillard, R. A., & McClintock, J. E. 2006, ARA&A, 44, 49
Reynolds, M. T., & Miller, J. M. 2011, ApJ, 734, L17
Reynolds, M. T., Reis, R. C., Miller, J. M., Cackett, E. M., & Degenaar, N. 2014, MNRAS, 441, 3656
Rybicki, G. B., & Lightman, A. P. 1979, Radiative Processes in Astrophysics (New York: Wiley-Interscience)
Shahbaz, T., Dhillon, V. S., Marsh, T. R., et al. 2005, MNRAS, 362, 975
Shakura, N. I., & Sunyaev, R. A. 1973, A&A, 24, 337
Sharma, P., Quataert, E., Hammett, G. W., & Stone, J. M. 2007, ApJ, 667, 714
Sironi, L., & Narayan, R. 2015, ApJ, 800, 88
Torres, M. A. P., Callanan, P. J., Garcia, M. R., et al. 2004, ApJ, 612, 1026
Wang, X., & Wang, Z. 2014, ApJ, 788, 184
Wrobel, J. M., Terashima, Y., & Ho, L. C. 2008, ApJ, 675, 1041
Wu, Q., Yuan, F., & Cao, X. 2007, ApJ, 669, 96
Xie, F.-G., Yang, Q.-X., & Ma, R. 2014, MNRAS, 442, L110 (XYM14)
Xie, F.-G., & Yuan, F. 2012, MNRAS, 427, 1580
Xie, F.-G., & Yuan, F. 2015, arXiv:1509. 02598 (MNRAS submitted)
Yang, Q.-X., Xie, F.-G., Yuan, F., et al. 2015, MNRAS, 447, 1692
Younes, G., Porquet, D., Sabra, B., Reeves, J. N., & Grosso, N. 2012, A&A, 539, A104
Yu, Z., Yuan, F., & Ho, L. C. 2011, ApJ, 726, 87
Yuan, F., & Cui, W. 2005, ApJ, 629, 408
Yuan, F., Cui, W., & Narayan, R. 2005, ApJ, 620, 905 (YCN05)
Yuan, F., Yu, Z., & Ho, L. C. 2009, ApJ, 703, 1034
Yuan, F., Bu, D., & Wu, M. 2012a, ApJ, 761, 130
Yuan, F., Wu, M., & Bu, D. 2012b, ApJ, 761, 129
Yuan, F., & Narayan, R. 2014, ARA&A, 52, 529
Yuan, F., Gan, Z., Narayan, R., et al. 2015, ApJ, 804, 101
Zdziarski, A. A., & Gierliński, M. 2004, Progress of Theoretical Physics Supplement, 155, 99
Zhang, J.-F., & Xie, F.-G. 2013, MNRAS, 435, 1165